From Sticky to Slippery Droplets: Dynamics of Contact Line Depinning on Superhydrophobic Surfaces

Wei Xu and Chang-Hwan Choi*

Department of Mechanical Engineering, Stevens Institute of Technology, Hoboken, New Jersey 07030, USA

(Received 1 April 2012; published 13 July 2012)

This study explores how surface morphology affects the dynamics of contact line depinning of an evaporating sessile droplet on micropillared superhydrophobic surfaces. The result shows that neither a liquid-solid contact area nor an apparent contact line is a critical physical parameter to determine the depinning force. The configuration of a contact line on a superhydrophobic surface is multimodal, composed of both two phases (liquid and air) and three phases (liquid, solid, and air). The multimodal state is dynamically altered when a droplet recedes. The maximal three-phase contact line attainable along the actual droplet boundary is found to be a direct and linear parameter that decides the depinning force on the superhydrophobic surface.

DOI: 10.1103/PhysRevLett.109.024504 PACS numbers: 47.55.D−, 47.55.dr, 47.55.np, 68.08.Bc

Patterned hydrophobic surfaces have attracted a lot of interest for their extreme water repellent property, typically exhibiting high contact angles for water droplets ($> 150°$) and they are called superhydrophobic [1,2]. Although the apparent contact angles on superhydrophobic surfaces are similar, they can be either slippery or sticky, differentiated by the pinning phenomena of the moving droplet on the surfaces. One example from nature is the phenomenon called the "lotus effect" vs "petal effect" [3]. On a lotus leaf, a water droplet rolls off very easily with little contact angle hysteresis. Such slippery surfaces have exhibited great applicability in self-cleaning [4], hydrodynamic friction reduction [5], anti-icing [6], anticorrosion [7], thermal or energy systems [8], biotechnology [9], and micro- and nanodevices [10]. Compared to the lotus leaf, a water drop on a petal surface does not roll off even if the petal surface is turned upside down. Such sticky superhydrophobic surfaces have potential applications in spraying or coating [11], ink-jet printing [12], liquid transportation and analysis [13], and microfluidic devices [14]. Therefore, it is of great significance to understand the physical mechanism of the pinning or depinning dynamics of a droplet on superhydrophobic surfaces for such tailored applications.

The pinning phenomena of droplets are affected by many surface parameters including chemical heterogeneity, physical structures, and interfacial wetting states [15–19]. As for superhydrophobic surfaces, the influence of surface structures on the droplet pinning has been studied from the perspective of both kinetics and dynamics [20–25]. However, the results are not consistent and the critical factor that would determine the pinning mechanics has not been clearly understood yet. Moreover, the direct mechanism of how the surface structures regulate the depinning dynamics on superhydrophobic surfaces has not been revealed much. In this Letter, we report an advanced understanding of the pinning or depinning mechanism on superhydrophobic surfaces by investigating an evaporating sessile droplet as a dynamics model, and propose a new physical criterion to evaluate the stickiness or slipperiness of superhydrophobic surfaces from the perspective of surface morphology.

When a droplet evaporates on a substrate, the droplet boundary is initially pinned to the substrate. Therefore, the contact radius of the droplet remains constant while the contact angle gradually decreases. Such a pinning mode then transits to a depinning mode with a decrease of contact radius, as illustrated in Fig. 1. The droplet pinning lasts until an initial quasiequilibrium contact angle reaches a receding contact angle. The unbalanced surface tension due to the change of contact angle results in the driving force for depinning motion of the droplet boundary, and the depinning force per unit length of the apparent droplet boundary can be expressed as [26]

$$F_d = \sigma(\cos\theta_r - \cos\theta_e), \tag{1}$$

where σ is the surface tension of liquid ($\sigma \simeq 72$ mN/m for water at 23 °C in this work), θ_r is a receding contact angle, and θ_e is an initial quasiequilibrium contact angle (Fig. 1).

To study the correlation between the structural parameters of a superhydrophobic surface and the depinning force,

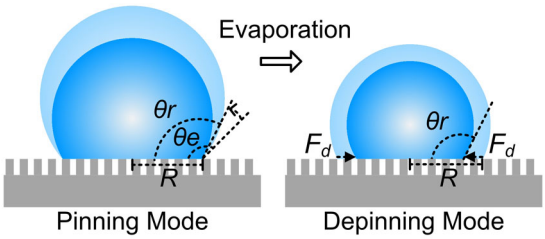

FIG. 1 (color online). The pinning and depinning phenomena of an evaporating droplet on a patterned superhydrophobic surface in a partial wetting (Cassie) state [28]. A pinning mode transits to a depinning mode during the evaporation process under the effect of a depinning force (F_d). θ_e is an initial quasiequilibrium contact angle, θ_r is a receding contact angle, and R is the contact radius of the droplet.

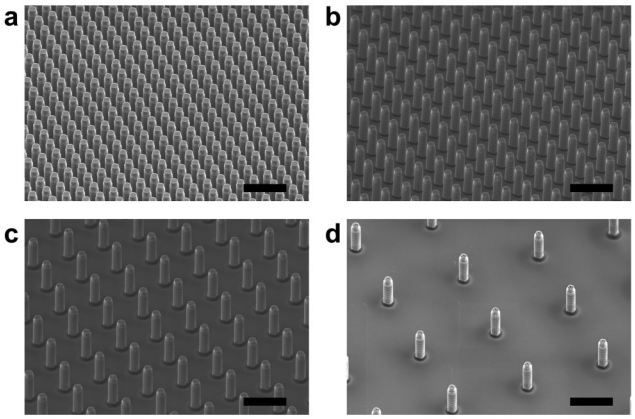

FIG. 2. Scanning electron microscopy images (45° tilted view) of the micropillared superhydrophobic surfaces. The liquid-solid contact area fraction in a partial wetting (Cassie) state varies from (a) 0.20, (b) 0.09, (c) 0.03, to (d) 0.01. Scale bars are 30 μm.

we prepared a square array of micropillars with systematically varied array densities on silicon substrates (Fig. 2) [27]. The micropillar patterns have the same diameter (5 μm) and height (25 μm), but different spaces between them (5, 10, 20, and 50 μm). After a Teflon hydrophobic coating, they make liquid droplets sit on the surfaces all in a partial wetting (Cassie) state with the contact angles greater than 150° [28], whereby the liquid-solid contact area fractions vary from 0.20, 0.09, 0.03, to 0.01, denoted as Φ0.20, Φ0.09, Φ0.03, and Φ0.01, respectively. A polished silicon substrate with a Teflon coating was also tested as a control, denoted as Φ1.00. Water droplets of ~4 μL were evaporated on the surface samples at a room condition (23 ± 1 °C, 32 ± 1% in humidity, and atmospheric pressure). The profiles of the evaporating droplets, including the contact angle and contact radius, were first measured with a goniometer system. Figure 3 shows the initial and

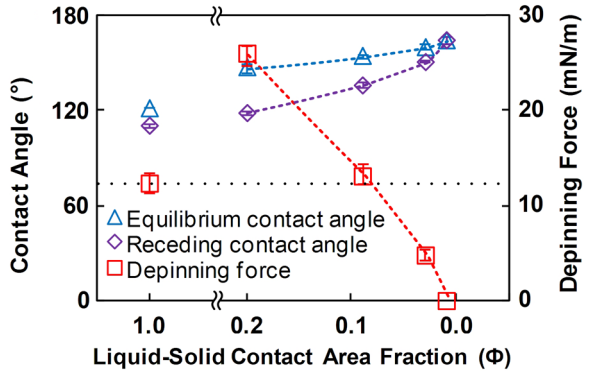

FIG. 3 (color online). The initial quasiequilibrium contact angles (θ_e), the receding contact angles (θ_r), and the depinning forces (F_d) on the patterned superhydrophobic surfaces (Φ0.20, Φ0.09, Φ0.03, and Φ0.01) and a planar hydrophobic surface (Φ1.00).

receding contact angles of a water droplet on each surface, and the resultant depinning forces calculated according to Eq. (1), with respect to the liquid-solid contact area fraction (Φ). The result shows that the depinning force declines dramatically with the decrease of the liquid-solid contact area. It even approaches zero on the Φ0.01 sample. However, the decrease rate is not linear with respect to the contact area (Φ). Moreover, on Φ0.20 and Φ0.09 samples, the depinning forces are greater than that on a planar surface (Φ1.00), despite the less liquid-solid contact area. It indicates that superhydrophobic surfaces can cause larger depinning force than a planar surface and the liquid-solid contact area fraction (Φ) is not a direct (linear) factor that determines the depinning force.

We further utilized a reflection interference contrast microscopy (RICM) technique to directly observe the droplet contact line and the liquid-solid interface (Fig. 4) [29]. For this experiment, transparent surface samples were prepared on polydimethylsiloxane (PDMS) substrates by replication [27]. Unlike the macroscopic apparent droplet boundary typically viewed as a simple circle, the RICM image reveals that the microscopic actual droplet boundary on the superhydrophobic surfaces is rugged and constituted by two parts: two-phase (liquid-air) and three-phase (liquid-solid-air) contact lines. During the evaporation process, the three-phase contact line at the droplet boundary is dynamically distorted [15]. Figures 5(a)–5(j) show the evolution of the actual droplet boundary during the evaporation. In the beginning, the three-phase contact line on most pillars occupies about 3/4 of the circular pillar perimeter [e.g., pillars *B* and *C* in Fig. 5(a)]. However, on the pillars where the droplet boundary veers off its direction across them [e.g., pillar *A* in Fig. 5(a)], the three-phase

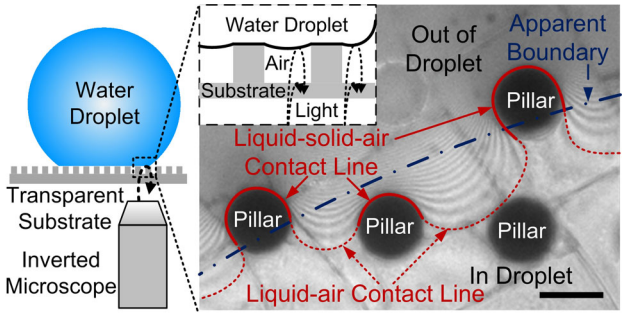

FIG. 4 (color online). The multimodal droplet boundary on a pillar-patterned superhydrophobic surface. The droplet boundary is observed from the backside of a transparent superhydrophobic substrate by using reflection interference contrast microscopy (RICM). The light reflected from the liquid-air interface and the substrate forms the interference fringe, which indicates the profile of liquid-air interface and locates the actual droplet boundary. This actual droplet boundary is different from the apparent boundary (drawn with the alternated long and short dash line), and is constituted by the three-phase (liquid-solid-air) contact line (shown by the solid line) and the two-phase (liquid-air) contact line (shown by the dash line). Scale bar is 20 μm.

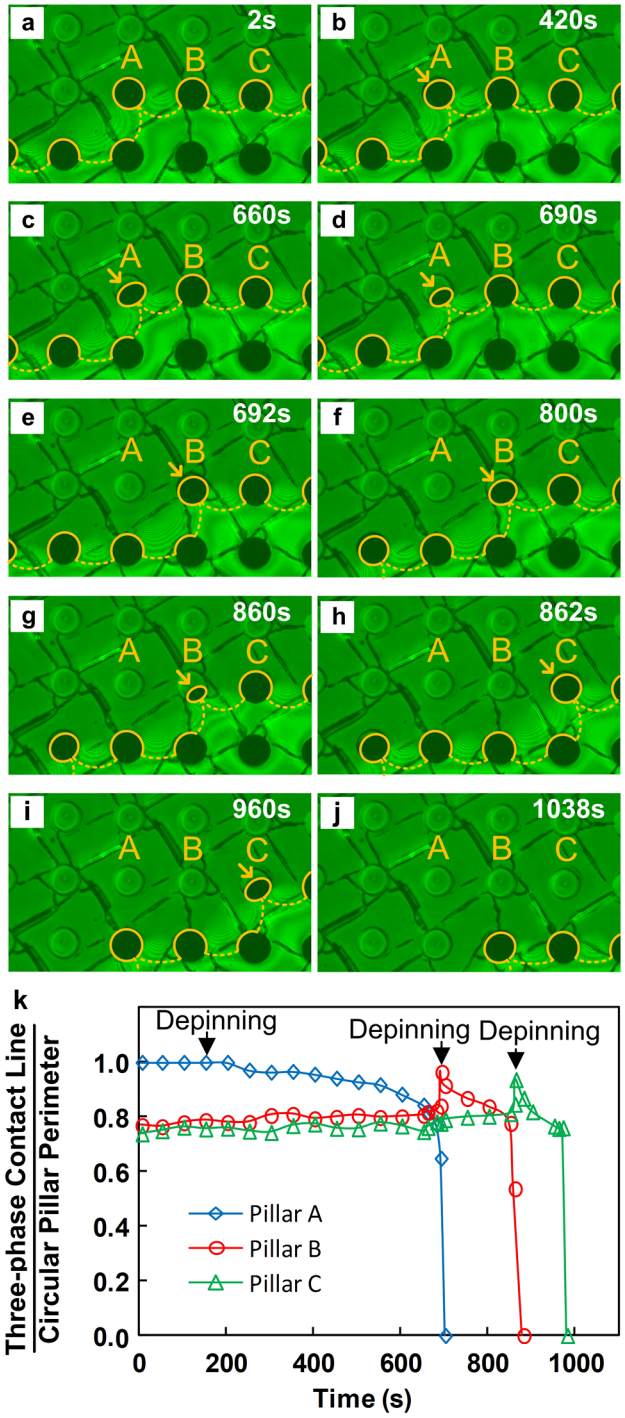

FIG. 5 (color online). The evolution of the actual boundary of an evaporating droplet on a micropillared superhydrophobic surface. The RICM images (a)–(j) show the sequential depinning progress from pillars A (a)–(d), B (e)–(g), and C (h)–(j), indicated by the arrows. The three-phase (liquid-solid-air) and the two-phase (liquid-air) contact lines on the droplet boundary are shown by the solid and dashed lines, respectively. (k) shows time history analysis of the normalized length ratio of the three-phase contact line to the circular pillar perimeter. It indicates that the depinning from each pillar initiates when the three-phase contact line reaches the maximum.

contact line elongates until it covers the whole periphery of the pillars. Then [e.g., after 420 s in Fig. 5(b)], the three-phase contact line begins to recede crossing the top surface of the pillars and eventually detaches. Figures 5(c)–5(j) show the sequential depinning progress of the three-phase contact line from pillars A to B to C [30]. Figure 5(k) summarizes the transitional progress in terms of the normalized length ratio of the three-phase contact line to the circular pillar perimeter. For pillar A, the normalized value remains constant during the pinning mode and then gradually decreases after depinning. For pillars B and C, it increases slowly in most of the pinning period, and then rapidly increases to the maximum (approximately unity, i.e., being equal to the circular perimeter of the pillar top) at the transition point from the pinning to depinning mode. After depinning, it abruptly drops to zero. Based on the observation that the onset of depinning occurs when the three-phase contact line reaches the maximum, we correlated depinning force to the maximal three-phase contact line. To account for varying droplet sizes, a maximal three-phase contact line normalized for an apparent droplet boundary is defined as

$$\delta = \frac{\sum_{i=1}^{n} l_i}{L_{\text{boundary}}}, \tag{2}$$

where n is the total number of the solid protrusions along the actual droplet boundary, l_i is the length of maximal three-phase contact line on the individual solid protrusion at the boundary, and L_{boundary} is the length of the macroscopic apparent droplet boundary (i.e., $2\pi R$). On the micropillared superhydrophobic surfaces, the maximal three-phase contact line on each circular pillar reached nearly equal to the perimeter of the top surface. In such a case, the normalized maximal three-phase contact line (δ) is reduced to

$$\delta = \frac{\pi d}{\lambda}, \tag{3}$$

where d is the diameter of a circular micropillar, and λ is the pitch between pillars. According to this analysis, the normalized maximal three-phase contact line (δ) for pillar-type structures is determined by the pitch between solid pillars (λ) and the perimeter of each pillar (πd).

Figure 6 shows the depinning force drawn for the new surface parameter δ on both the superhydrophobic surfaces and a planar hydrophobic surface. The result shows that the depinning force exhibits good linearity with δ. On a planar surface (Φ1.00), the δ is equal to unity since the length of maximal three-phase contact line is the same as the perimeter of a droplet boundary. On superhydrophobic surfaces, when δ is greater than unity, such as for the Φ0.20 and Φ0.09 samples, a higher depinning force is observed than that on a planar hydrophobic surface. It suggests that the micropillared superhydrophobic surfaces of $\delta > 1$ behave as a stickier surface than a planar hydrophobic

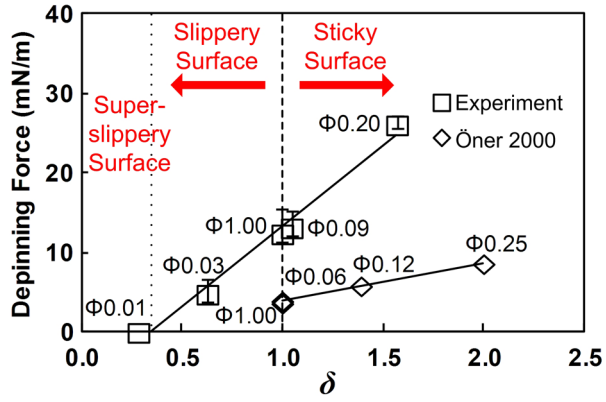

FIG. 6 (color online). The linear correlation between the depinning force and the normalized maximal three-phase contact line (δ) at the droplet boundary. Linearly depending on the surface parameter δ, the superhydrophobic surfaces behave as sticky, slippery, or superslippery surfaces, compared to a planar hydrophobic surface. The result from Öner *et al.* [23] has been analyzed [33] with the new parameter δ for comparison.

surface. On the contrary, if δ is less than unity, such as $\Phi 0.03$ and $\Phi 0.01$ samples, a lower depinning force is measured on the superhydrophobic surfaces, suggesting that the micropillared superhydrophobic surfaces of $\delta < 1$ turn to be slippery compared to a planar hydrophobic surface. McCarthy *et al.* have commented on the importance of the three-phase contact line and its pinning effect on contact angle hysteresis (the difference between advancing and receding contact angles) [23–25]. However, the three-phase contact line referred to in their study represents a static and apparent one, instead of a dynamic and actual three-phase contact line. Such static and apparent surface parameters are inappropriate to understand the dynamic behaviors of the contact line depinning on the superhydrophobic surfaces that impose the multimodal multiphase boundary conditions. Therefore, no direct (linear) correlation between the surface structures and surface stickiness could be revealed in their study. For comparison, we examined their experimental data [23] in terms of our new parameter δ, which is also plotted in Fig. 6. Then, they now show a good linear correlation between the depinning force and δ. This further confirms and validates the linear dependency of the depinning force on the new parameter δ. In Fig. 6, the different slopes fitted to the data reflect the different intrinsic surface property (e.g., initial and receding contact angles) of the hydrophobic coatings used in the works (Teflon coating was used in this work, while dimethyldichlorosilane in Öner's experiment).

On the other hand, McHale *et al.* reported no significant change in the contact angle hysteresis, when the contact perimeter of the liquid-solid interface was varied but the effective contact area of the liquid-solid interface was held constant. Based on the observation, they concluded that the contact angle hysteresis should be a consequence of the effective contact area between liquid and solid [20,21]. However, such conclusion cannot explain the results exhibited in this study, that the depinning forces can be even greater on certain superhydrophobic surfaces (i.e., $\Phi 0.20$ and $\Phi 0.09$ samples) than that on a planar surface (i.e., $\Phi 1.00$). We also analyzed their data [20,21] in terms of the new parameter δ. We found that their surface samples were made to have the same δ value accidentally. According to the new criterion discovered in this study, the surface morphologies that have the same δ value should result in the same depinning force and so for the contact angle hysteresis. Thus, the experimental results of McHale *et al.* [20,21] also turn out to agree with the new linear criterion to δ. All these results support that the normalized maximal three-phase contact line along the actual droplet boundary of multimodes is the direct (linear) factor determining the pinning/depinning dynamics on the superhydrophobic surfaces rather than other parameters describing the surface and interfacial morphology such as static or apparent contact line and contact area.

By investigating the geometric profile and contact interface of an evaporating sessile droplet on micropillared superhydrophobic surfaces, this study reveals the dynamic mechanism of the contact line depinning of receding droplets and its direct correlation to the surface morphology of superhydrophobic surfaces. The depinning force, which drives the movement of droplet boundary, is found to display a linear correlation with the normalized maximal three-phase contact line at the droplet boundary, which depends on the morphology of the surface structures. This new insight paves the way to better understand the outstanding problem of interfacial wetting, adhesion, and frictional properties on textured surfaces, such as pinning, slip, and contact angle hysteresis. Not only for droplet dynamics, the depinning of the three-phase contact line is also of significant importance in the friction reduction in continuous flows. The contact line depinning facilitates the separation of the liquid flow from the solid surface so that it can provide more air fraction on the surface and result in an enhanced slip and friction reduction [31]. Another example is unidirectional wetting, pinning, and spreading phenomena on patterned surfaces [18,19]. The new surface parameter revealed in this study will benefit the understanding of such phenomena from the perspective of anisotropic maximal three-phase contact line, as well as the function of other anisotropically textured surfaces in nature, such as the legs of a water strider, wings of a butterfly, and leaves of a plant [32]. Such advanced understanding of the dynamics of contact line depinning on structured surfaces can offer essential guidelines for the engineering of versatile superhydrophobic surfaces that can regulate their slipperiness and stickiness tailored to particular and customized applications with broader impact.

This research was carried out in part at the Center for Functional Nanomaterials, Brookhaven National Laboratory, which was supported by the U.S. Department

of Energy, Office of Basic Energy Sciences, under Contract No. DE-AC02-98CH10886. The research effort used microscope resources partially funded by the National Science Foundation through NSF Grant No. DMR-0922522.

*Corresponding author.
Chang-Hwan.Choi@stevens.edu

[1] A. Lafuma and D. Quéré, Nature Mater. **2**, 457 (2003).
[2] H. Y. Erbil, A. L. Demirel, Y. Avcı, and O. Mert, Science **299**, 1377 (2003).
[3] L. Feng, Y. Zhang, J. Xi, Y. Zhu, N. Wang, F. Xia, and L. Jiang, Langmuir **24**, 4114 (2008).
[4] R. Fürstner, W. Barthlott, C. Neinhuis, and P. Walzel, Langmuir **21**, 956 (2005).
[5] C.-H. Choi and C.-J. Kim, Phys. Rev. Lett. **96**, 066001 (2006).
[6] K. K. Varanasi, T. Deng, J. D. Smith, M. Hsu, and N. Bhate, Appl. Phys. Lett. **97**, 234102 (2010).
[7] P. M. Barkhudarov, P. B. Shah, E. B. Watkins, D. A. Doshi, C. J. Brinker, and J. Majewski, Corros. Sci. **50**, 897 (2008).
[8] J. B. Boreyko and C.-H. Chen, Phys. Rev. Lett. **103**, 184501 (2009).
[9] C.-H. Choi and C.-J. Kim, Langmuir **25**, 7561 (2009).
[10] W. Xu, R. Leeladhar, Y.-T. Tsai, E.-H. Yang, and C.-H. Choi, Appl. Phys. Lett. **98**, 073101 (2011).
[11] I. B. Rietveld, K. Kobayashi, H. Yamada, and K. Matsushige, J. Phys. Chem. B **110**, 23351 (2006).
[12] P. Calvert, Chem. Mater. **13**, 3299 (2001).
[13] X. Hong, X. Gao, and L. Jiang, J. Am. Chem. Soc. **129**, 1478 (2007).
[14] W. K. Cho and I. S. Choi, Adv. Funct. Mater. **18**, 1089 (2008).
[15] P. S. H. Forsberg, C. Priest, M. Brinkmann, R. Sedev, and J. Ralston, Langmuir **26**, 860 (2010).
[16] C. Priest, R. Sedev, and J. Ralston, Phys. Rev. Lett. **99**, 026103 (2007).
[17] M. Liu, Y. Zheng, J. Zhai, and L. Jiang, Acc. Chem. Res. **43**, 368 (2010).
[18] K.-H. Chu, R. Xiao, and E. N. Wang, Nature Mater. **9**, 413 (2010).
[19] N. A. Malvadkar, M. J. Hancock, K. Sekeroglu, W. J. Dressick, and M. C. Demirel, Nature Mater. **9**, 1023 (2010).
[20] G. McHale, N. J. Shirtcliffe, and M. I. Newton, Langmuir **20**, 10146 (2004).
[21] N. J. Shirtcliffe, S. Aqil, C. Evans, G. McHale, M. I Newton, C. C. Perry, and P. Roach, J. Micromech. Microeng. **14**, 1384 (2004).
[22] C. W. Extrand, Langmuir **18**, 7991 (2002).
[23] D. Öner and T. J. McCarthy, Langmuir **16**, 7777 (2000).
[24] L. Gao and T. J. McCarthy, Langmuir **22**, 6234 (2006).
[25] K. A. Wier and T. J. McCarthy, Langmuir **22**, 2433 (2006).
[26] K. Sefiane, J. Colloid Interface Sci. **272**, 411 (2004).
[27] See Supplemental Material at http://link.aps.org/supplemental/10.1103/PhysRevLett.109.024504 for the fabrication process of micropatterned superhydrophobic surfaces.
[28] A. B. D. Cassie and S. Baxter, Trans. Faraday Soc. **40**, 546 (1944).
[29] S. Moulinet and D. Bartolo, Eur. Phys. J. E **24**, 251 (2007).
[30] See Supplemental Material at http://link.aps.org/supplemental/10.1103/PhysRevLett.109.024504 for the video showing the contact line depinning of an evaporating droplet.
[31] P. Gao and J. J. Feng, Phys. Fluids **21**, 102102 (2009).
[32] X. Gao and L. Jiang, Nature (London) **432**, 36 (2004).
[33] In the analysis of the data previously reported by Öner and McCarthy, the quasiequilibrium contact angle on a planar surface was calculated as the average of the advancing and the receding contact angles. The initial apparent contact angles on their superhydrophobic surfaces were calculated according to the Cassie-Baxter equation.